Self-assembly of Peptide−Amphiphile C_{12}−Aβ(11−17) into Nanofibrils

Manli Deng, Defeng Yu, Yanbo Hou, and Yilin Wang*

Beijing National Laboratory for Molecular Sciences, Key Laboratory of Colloid and Interface Science, Institute of Chemistry, Chinese Academy of Sciences, Beijing 100190, People's Republic of China

Received: April 22, 2009

A peptide−amphiphile (C_{12}−Aβ(11−17)) was constructed with a key fragment of amyloid β-peptide (Aβ(11−17)) attached to dodecanoic acid through an amide bond. The self-assembly behavior of C_{12}−Aβ(11−17) in aqueous solution is studied at 25 °C and at pH 3.0 and 10.0. Aβ(11−17) cannot form ordered self-assemblies. But C_{12}−Aβ(11−17) exhibits a very strong ability to form ordered nanofibrils, and the specific fine structure of the nanofibrils can be modulated simply by adjusting the concentration or pH. The critical micelle concentration of C_{12}−Aβ(11−17) was determined as 0.063 and 0.11 mM at pH 3.0 and 10.0, respectively, indicating a stronger assembling ability of C_{12}−Aβ(11−17) at acidic pH. In 0.47 mM C_{12}−Aβ(11−17) solution at pH 3.0, rodlike fibrils with a diameter of ∼5 nm and varying length of hundreds of nanometers are observed. When the C_{12}−Aβ(11−17) concentration increases to 1.87 mM at pH 3.0, the above rodlike fibrils pack in parallel and form tapelike fibrils through lateral association. In 1.87 mM C_{12}−Aβ(11−17) solution at pH 10.0, twisted fibrils with regular periodicity of ∼200 nm are formed by the twisting of ∼20 nm wide and ∼11 nm thick nanoribbons. The hydrophobic moiety is necessary in fibril formation, whereas the β-sheet secondary structure of the peptide moiety plays an essential role in the twisting morphology. This work helps to understand the possible mechanism in amyloid fibrillogenesis and provides an approach to inscribe biological signals in self-assemblies with potential application in biomaterial fabrication.

Introduction

Self-assembly of peptide-based amphiphiles have recently emerged as one of the most promising scaffolding for nano-/microscale biomaterials in tissue engineering[1−3] and other medical applications such as regenerative medicine[4,5] and controlled drug release.[6] Various classes of peptide-based amphiphiles have been reported, including amphiphilic peptides[7−10] and peptide−amphiphiles.[11−14] Amphiphilic peptides are usually constructed with hydrophobic and hydrophilic amino acid residues, including the structures of a charged head attached to a nonpolar tail,[15−17] alternating positive/negative[6,9] or polar/nonpolar[7,18,19] amino acid repeat units, and well-designed α-helix with hydrophilic and hydrophobic faces.[20,21] These chemical sequences lead to aggregates of different hierarchies ranging from vesicle to nanotubes, and from twisted ribbons to fibril networks. Peptide−amphiphile is a kind of synthetic surfactant that typically contains one or more long alkyl chains attached to a peptide moiety. It has been found that many peptide−amphiphiles assemble into nanofibers in aqueous solution, structurally similar to cylindrical micelles, in which the alkyl tails bury in the core of the fibers while the hydrophilic oligopeptides pack on the fiber's surface. The interactions that lead to the formation of these structures include chiral dipole−dipole interaction, $\pi-\pi$ stacking, hydrogen bond, nonspecific van der Waals interaction, hydrophobic force, electrostatic interaction, and repulsive steric force. All systems studied involved combinations of these forces that counterbalance the enormous translational and rotational entropic cost caused by poly molecular aggregation.[22] Particularly, the β-sheet formation between the peptide regions of peptide−amphiphile molecules has been recognized as a predominant factor in directing the self-assembly into cylindrical architecture as opposed to spherical micelles or vesicles.[15,23,24]

Amyloid β-peptide (Aβ), a 39−43-residue amphiphilic peptide, is the major component of the neuritic plaques found in the brains of patients suffering from Alzheimer's disease. The secondary structure conversion from random coil or α-helix to β-sheet conformation has been proposed as one of the critical reasons for the peptide fibrillogenesis and neurotoxicity.[25] Earlier studies[26,27] have demonstrated that the trifluoroethanol-stabilized monomeric Aβ(1−42) delineated two separated helical domains, but only the destabilization of helix I, comprising residues 11−24, caused a transition to a β-sheet structure and a consequent amyloid formation. Therein, the hydrophobic region between positions 17 and 21 makes up the β-sheet core of the amyloid fibrils,[28,29] and Aβ(16−22) is the smallest fragment of Aβ known to form fibrils.[8,30] The most stable helical region is located between positions 11 and 17,[27] which significantly contributes to the stability of the α-helical secondary structure of Aβ and the inhibition of peptide fibrillogenesis.

Herein, the Aβ fragment of residues 11−17 (EVHHQKL) is taken as the head group of a peptide−amphiphile. The introduction of Aβ(11−17) endows the desired molecule with biological features, while the alkyl chain attached onto the *N*-terminal of Aβ(11−17), serving as the hydrophobic region 17−21 of Aβ, facilitates the molecular assembly. The chemical structure and space-filling model of the designed peptide−amphiphile (C_{12}−Aβ(11−17)) are shown in Figure 1. The pH and concentration dependence of C_{12}−Aβ(11−17) self-assembly in aqueous solution are investigated by isothermal titration microcalorimetry, ζ-potential, circular dichroism, atomic force microscopy, and transmission electron microscopy.

* To whom correspondence should be addressed. E-mail: yilinwang@iccas.ac.cn.

10.1021/jp904289y CCC: $40.75
Published on Web 06/01/2009

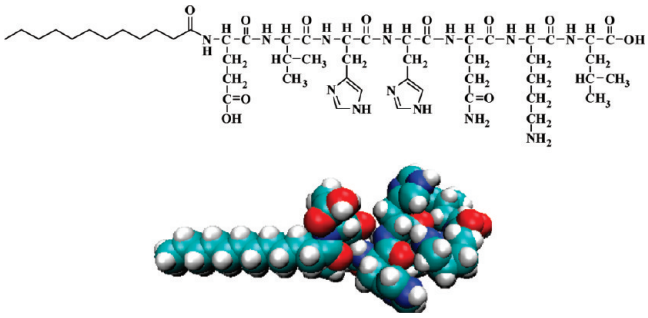

Figure 1. Chemical structure and space-filling model of peptide−amphiphile C_{12}−Aβ(11−17), with a peptide sequence of EVHHQKL from N- to C-terminal.

Experimental Section

Material. The heptapeptide Aβ(11−17) was purchased from GL Biochem (Shanghai) Ltd. We designed peptide−amphiphile C_{12}−Aβ(11−17) and its synthesis was carried out by GL Biochem (Shanghai) Ltd. The purities of Aβ(11−17) and C_{12}−Aβ(11−17) were checked by high-performance liquid chromatography (better than 98%). The inorganic reagents (>99.5%) were purchased from Beijing Chemical Co. Milli-Q water (18 M$\Omega\cdot$cm^{-1}) was used throughout.

Sample Preparation. An appropriate amount of C_{12}−Aβ(11−17), with a molecular weight of 1072.30, was dissolved in water to obtain the desired concentration, and then the solution was vortex-mixed. The pH was adjusted with concentrated HCl or NaOH solution to achieve the desired values.

Isothermal Titration Microcalorimetry (ITC). The calorimetric measurements were taken in a TAM 2277-201 microcalorimetric system (Thermometric AB, Järfälla, Sweden) with a 1 mL stainless steel sample cell at 25.00 ± 0.01 °C. The cell was initially loaded with 0.6 mL of water of pH 3 or 10. Each aliquot of 8 μL of concentrated C_{12}−Aβ(11−17) solution at the corresponding pH was injected consecutively into the stirred sample cell via a 500 μL Hamilton syringe controlled by a 612 Thermometric Lund pump until the desired concentration range had been covered. The interval between two injections was 10 min, which was long enough for the signal to return to the baseline. The observed enthalpy (ΔH_{obs}) was obtained by integrating the areas of the peaks in the plot of thermal power against time.

ζ-Potential Measurements. The ζ-potential measurements were performed at 25.0 ± 0.1 °C using a Malvern Zetasizer Nano-ZS instrument (ZEN3600, Malvern Instruments, Worcestershire, UK) equipped with a 4 mW He−Ne laser at a wavelength of 633 nm.

Circular Dichroism. Circular dichroism (CD) spectra were recorded on a JASCO J-815 spectrophotometer at room temperature using a 0.1 mm quartz cell. Scans were obtained in a range between 190 and 260 nm by taking points at 0.5 nm, with an integration time of 0.5 s. Five spectra were averaged to improve the signal-to-noise ratio and smoothed using the noise-reducing option in the software supplied by the vendor. The results were represented as machine unit (θ, in units of mdeg).

X-ray Diffraction. Self-supported cast films were prepared by dispersing the aqueous solutions of C_{12}−Aβ(11−17) onto precleaned silicon wafers and then dried under vacuum. Reflection X-ray diffraction (XRD) studies were carried out with an X-ray diffractometer (XRD-7000, Shimadzu, Japan). The X-ray beam was generated with a Cu anode at 40 kV and 30 mA, and the wavelength of the $K_{\alpha 1}$ beam was 1.5406 Å. The X-ray beam was directed to the edge of the film, and the scanning 2θ was recorded from 1 to 15°, using a step width of 0.02°.

TABLE 1: Values of CMC, ΔH_{mic}, and ζ-Potential for the C_{12}−Aβ(11−17) Solution of pH 3.0 and pH 10.0 at 25.0 °C

	CMC (mM)	ΔH_{mic} (kJ/mol)	ζ-potential (mV)
pH 3.0	0.063	13.51	49.8
pH 10.0	0.109	5.08	−54.2

Atomic Force Microscopy. For ambient atomic force microscopy (AFM) imaging, 10 μL of C_{12}−Aβ(11−17) solution was deposited onto a freshly cleaved piece of mica and left to adhere for 10 min. The sample was then rinsed with 100 μL of water and dried with a gentle stream of nitrogen. AFM imaging was performed at room temperature using the tapping mode on a Multimode Nanoscope IIIa AFM (Digital Instruments, CA). Probes used are etched silicon probes with a typical tip radius of ~10 nm, attached to 125 μm cantilevers with a nominal spring constant of 40 N/m (Digital Instruments, model RTESPW). All images were acquired with a scan speed of 1.0−1.5 Hz, a tip resonance frequency of 230−300 kHz, and a drive amplitude of 20−100 mV. Height data were collected as 512 × 512 pixel images. Topographic data were regularly recorded in both trace and retrace to check on scan artifacts. Analysis of the images was carried out using the Digital Instruments Nanoscope software (version 512r2). In each case, at least 50 individual fibrils from different samples were analyzed at different parts.

Transmission Electron Microscopy. Transmission electron microscopy (TEM) samples were prepared from C_{12}−Aβ(11−17) solutions using negative-staining method, and 1% uranyl acetate solution was used as the staining agent. A drop of the solution was placed onto a carbon Formvar-coated copper grid, and the excess liquid was sucked away by filter paper. After drying, the samples were imaged under an electron microscope (FEI Tecnai 20).

Results and Discussion

Since peptide−amphiphile C_{12}−Aβ(11−17) is pH-sensitive, two pHs, 3.0 and 10.0, were selected to define the protonation states of the C_{12}−Aβ(11−17) molecules in aqueous solution. The pK_a values of the carboxylic group in Leu and in the side chain of Glu, the imidazolyl group in His, and the pK_b value of the amino group in Lys are 2.36, 4.25, 6.00, and 10.53, respectively.[13] Thus, the peptide−amphiphile molecule carries approximately two positive net charges at pH 3.0 but two negative net charges at pH 10.0. This can be verified by the comparable absolute values of the ζ-potential values for the 1.87 mM C_{12}−Aβ(11−17) solution at the two pHs, as presented in Table 1.

ITC measurements were conducted at 25.00 °C to determine the critical micelle concentrations (CMC) of C_{12}−Aβ(11−17) at pH 3.0 and 10.0, respectively. Actually, the self-assemblies of C_{12}−Aβ(11−17) in aqueous solution have irregular micellar morphology, referring to the following part of the discussion. The present CMC is used to describe the formation of any structure with micellar characteristics. The calorimetric titration curves of the observed enthalpy (ΔH_{obs}) are plotted against the final C_{12}−Aβ(11−17) concentration (C) in Figure 2. The CMC can be identified as the extreme of the differentiating observed enthalpy curve with respect to C. The apparent enthalpy change of micellization (ΔH_{mic}) is obtained from the enthalpy difference between the two linear segments of the enthalpy curve extrapolated to the CMC (Table 1). The slightly smaller CMC in the acidic solution indicates the stronger assembling ability of

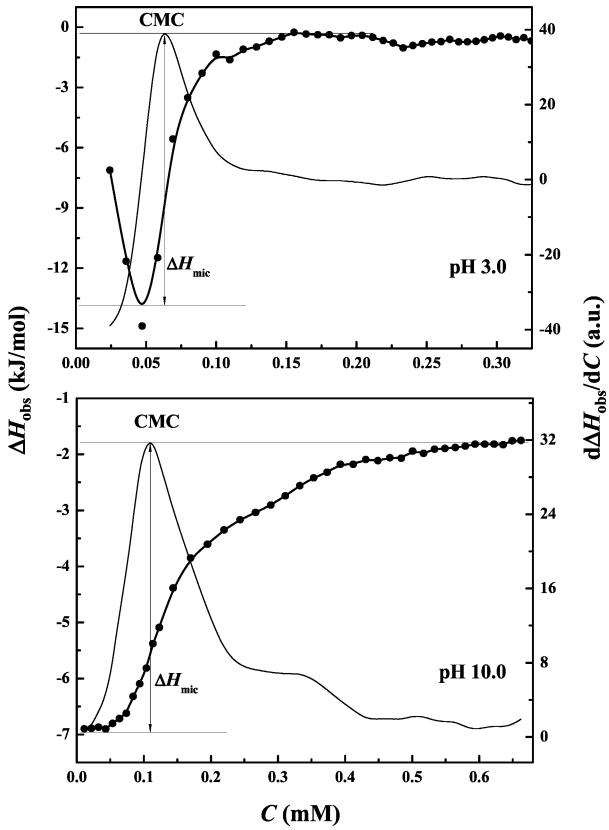

Figure 2. Variation of the observed enthalpy (ΔH_{obs}) with the final C_{12}−Aβ(11−17) concentration (C) at 25.00 ± 0.01 °C and at pH 3.0 and 10.0.

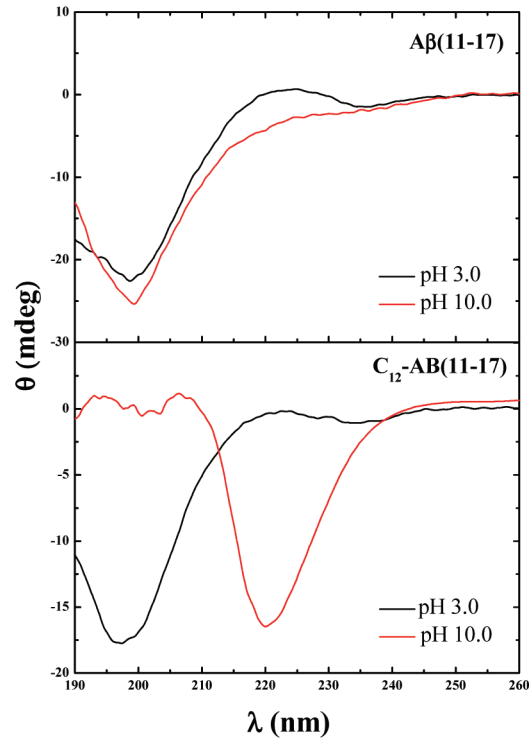

Figure 3. CD spectra of Aβ(11−17) and C_{12}−Aβ(11−17) solutions at pH 3.0 and 10.0.

C_{12}−Aβ(11−17) at pH 3.0. The ΔH_{mic} is endothermic at both acidic and alkaline conditions, suggesting the micellization is an entropy-driven process. The endothermic ΔH_{mic} should be mainly contributed from the electrostatic repulsion between the C_{12}−Aβ(11−17) molecules with either positive or negative charges as well as the dehydration effect accompanied by the formation of the hydrogen bond between the amino acid residues. In addition, the much less endothermic ΔH_{mic} at pH 10.0 implies that the corresponding micellization process may involve less strong intermolecular repulsions with respect to that at pH 3.0.

To characterize the secondary structure of the C_{12}−Aβ(11−17) assemblies, CD measurements were performed at room temperature for 1.87 mM C_{12}−Aβ(11−17) solutions at pH 3.0 and 10.0 and the Aβ(11−17) solutions at the same conditions (Figure 3). The 2.2 mM Aβ(11−17) solutions at pH 3.0 and 10.0 were both found to be a random coil secondary structure signaled by the minimum around 198 nm. That is to say, the pH does not affect the secondary structure of Aβ(11−17). In the case of 1.87 mM C_{12}−Aβ(11−17), the self-assemblies formed at pH 3.0 inherit the random coil secondary structure of the peptide sequence, but at pH 10.0, the self-assemblies display a typical β-sheet secondary structure as a single minimum at approximately 220 nm. These results suggest both the introduction of the C_{12} alkyl chain and the change in pH affect the peptide secondary structure. At pH 3.0, the C_{12}−Aβ(11−17) molecules could assemble through hydrophobic interaction at the concentration used, but the two positively charged His residues in the middle of the head group enhance the electrostatic repulsion to prevent the formation of ordered secondary structure. At pH 10.0, besides the hydrophobic interaction among the alkyl chains, the disappearance of repulsion between intermolecular His residues facilitates the hydrogen bonding within the whole peptide moiety, which induces the formation of the β-sheet secondary structure. This preference has also been suggested by the value of ΔH_{mic} at these two pH conditions.

The difference in the secondary structure of the peptide moiety at different pHs may play a crucial role in the assembly morphology of the peptide amphiphile. To identify the morphology of the C_{12}−Aβ(11−17) self-assemblies, complementary AFM and TEM were carried out on its aqueous solutions at different concentrations above CMC and at different pHs. The corresponding heptapeptide fragment Aβ(11−17) was first studied for comparison. All the sample solutions were incubated at 25.0 ± 0.5 °C for at least 24 h before imaging to achieve the stable assembly states.

As shown in Figure 4, only small spherical self-assemblies are observed for 2.2 mM Aβ(11−17) at both pHs. The heights of these self-assemblies range from 1 to 5 nm, which should be the peptide oligomers.[32] The morphology remains unchanged for more than 3 weeks after the solution preparation. That Aβ(11−17) could not organize into ordered assemblies may be attributed to its lack of hydrophobic interaction and the consequent weak self-assembly ability.

Figure 5 presents the morphologies of the C_{12}−Aβ(11−17) assemblies formed at 0.47 and 1.87 mM, at pH 3.0 and 10.0, respectively. The assemblies exhibit fibril morphology at all the conditions, but vary remarkably in fine structures depending on both concentration and pH.

In 0.47 mM C_{12}−Aβ(11−17) solution at pH 3.0, rodlike nanofibrils are observed in the AFM image (Figure 5A_2), with an average height of 2.5 ± 0.5 nm and varying length from about 50 to 200 nm. The height value is very close to the calculated length of a C_{12}−Aβ(11−17) molecule, so the observed assembles on mica is possibly the collapsed C_{12}−Aβ(11−17) cylindrical micelles. Meanwhile, the fibrils observed in TEM image (Figure 5A_1) are a little larger in

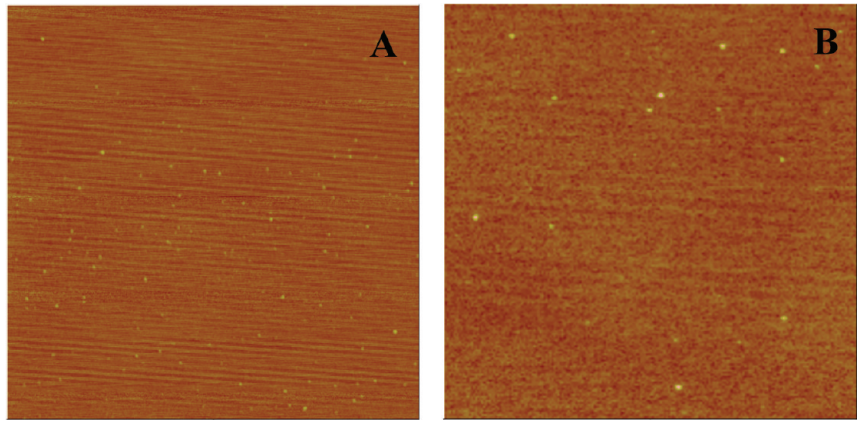

Figure 4. Morphologies of 2.2 mM Aβ(11−17) at (A) pH 3.0 and (B) pH 10.0. Both of the images are 2 × 2 μm^2 in size and 5 nm in height.

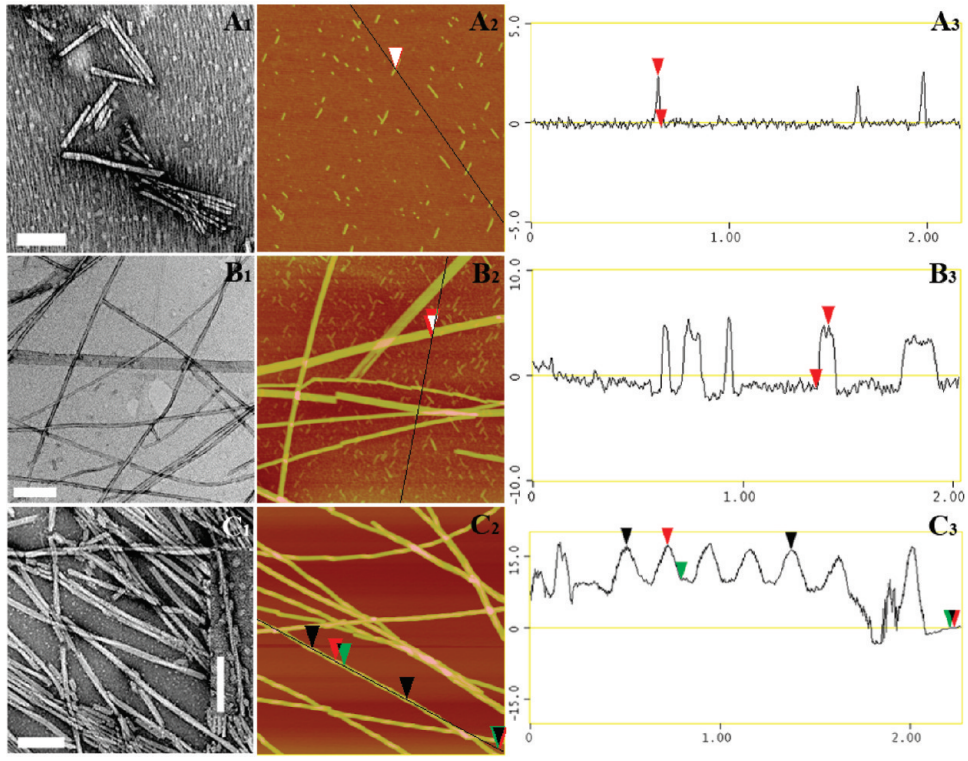

Figure 5. From left to right are the TEM images, AFM height images, and section analyses of the C_{12}−Aβ(11−17) assemblies at different concentrations and pHs: (A) 0.47 mM, pH 3.0; (B) 1.87 mM, pH 3.0; and (C) 1.87 mM, pH 10.0. All the AFM images are 2 × 2 μm^2 in size, and the scale bars represent 200 nm in all TEM images.

dimension with a 10−30 nm width and 100−400 nm length. And it can be seen from the terminals of these fibrils that each one is composed of two or more cylindrical micelles by bundling together. The difference in morphology between AFM and TEM images may be from the drying process. The AFM sample was rinsed with water before drying; thus, the assemblies were highly dispersed. Contrarily, there was condensation during drying of the TEM sample in which the assemblies tended to aggregate. This effect is particularly remarkable for the assemblies in small size, which has a relatively high diffusion coefficient in aqueous solution and is very sensitive to the concentration.

Compared with the situation of Aβ(11−17), the primary driven force of the C_{12}−Aβ(11−17) self-assembly should be hydrophobic interaction between the alkyl chains of the peptide−amphiphile molecules. The cylindrical micelle of C_{12}−Aβ(11−17) should be constructed by the hydrophobic alkyl tails emerging into the core region and leaving the hydrophilic peptide moieties exposed to water. But the high aspect ratio of the micelle geometry should be attributed to the hydrogen bonds between the peptide moieties. The importance of hydrogen bonds in the formation of nanofibrils has been recognized and emphasized in the literature.[12,19,33] A systematic study[11] has been performed on a series of peptide−amphiphiles with a seven-glycine linker region localized between an alkyl tail and a four-residue head group. It was pointed out that the formation of the hydrogen bonds close to the hydrophobic alkyl tails is the necessary controlling factor in the formation of cylindrical shape. In the present system, the assembled alkyl chains could generate the possibilities of intermolecular hydrogen bonds between the nearby amino acid residues (such as Glu and Val), which may lead to the observed cylindrical geometry of the self-assemblies, though no β-sheet structure formed.

To clarify the concentration dependence of the assembly morphology, TEM and AFM measurements were also performed on 1.87 mM C_{12}−Aβ(11−17) solution at the same pH, i.e., 3.0. Quite long fibrils, up to micrometers, are observed (Figure 5B).

As clearly seen from Figure 5B_2, the long fibrils are coexisting with short fibrils in the background, identical to that formed at 0.47 mM. It implies that the increase in the micelle's concentration may drive the C_{12}−Aβ(11−17) cylindrical micelles to grow from low-order (short) fibrils into high-order (long) fibrils through hydrogen bonding in larger scale. Besides, it is noted that high-order fibrils, with length of hundreds of nanometers, consecutively adsorbed on the substrate (in the middle of the AFM image), signaling the rigid nature of the fibrils formed at pH 3.0. However, the major distinction between the high-order and low-order fibrils is the height, whose value of the former is at least 2 times that of the latter. Thus, the high-order fibrils might be assembled from the elongated cylindrical C_{12}−Aβ(11−17) micelles without breakdown on mica. Two predominant morphologies of the high-order fibrils are observed from both TEM and AFM images, the filaments of 5−15 nm in width and the nanotapes above 50 nm in width. Both of them should be constructed by the lateral association of the cylindrical micelles in varying numbers, as occurred in the amyloid fibrillogenesis.[32] Because the micelle surface is covered by three residues (Gln, Lys, and Leu) at the C-terminal, which are nonionic at pH 3.0 and are prone to form hydrogen bonds not only in the backbones but also in the side chains, the micelles could draw close to each other and bind through hydrogen bonds. That is to say, the high-order fibrils are fabricated by a hydrogen bond network, which plays a crucial role in the assembly geometry and in further association of the primary assemblies.

To know the pH dependence of the assembly morphology, TEM and AFM measurements were then performed on the 1.87 mM C_{12}−Aβ(11−17) solution at pH 10.0. Distinctive morphology of the fibrils are seen (Figure 5C). Different from the fibrils at pH 3.0, all the fibrils at pH 10.0 are in a regular twisting conformation and some of them entwine with each other. The handedness of the fibrils seems random, either left-handed or right-handed within each individual. Oda et al.[34] discriminated the twisting assemblies into helical ribbons with a cylindrical curvature from twisted ribbons with a Gaussian or saddlelike curvature. In the present case, fibrils in various twisting conformations coexist (Figure 5C_1), and the twisting ribbons should be the predominant category. Baumann et al.[35] revealed that, for short amphiphilic peptides, β-sheet secondary structure correlates with ribbonlike assemblies while random coil structure correlates with rodlike assemblies. Here, it could be assumed that the ribbon is constructed by the β-sheet secondary structure of the C_{12}−Aβ(11−17) peptide moiety. The peptide backbones form intermolecular hydrogen bonds perpendicular to the ribbon's long axis. And each β-stand would pack with the next one along the ribbon's long axis in a small twisting angle as a result of the steric hindrance of the amino acid side chains (such as the imidazolyl group), which cause the ribbon to twist. From the TEM image, the average values of the thickness, the width, and the twisting periodicity of the twisting ribbon were measured as 12 ± 1, 19 ± 1, and 200 ± 10 nm, respectively. Of particular, the AFM image (Figure 5C_2) shows perfect twisting periodicity for most of the fibrils, as obviously seen from the section analysis in profile along the fibril long axis. The periodicity can be measured from the horizontal distance of the two neighboring peaks or the average of a number of the peaks, as marked by the black arrows. Because the magnitude of the periodicity is far larger than the assemble height, the AFM tip-related convolution effect could be neglected. The mean value is obtained as 190 ± 15 nm, in good agreement with the value from the corresponding TEM images. Moreover, the vertical distances between the red arrows and between the green arrows respectively characterize the altitudes of the protuberant part and the sunk part of the twists with respect to the substrate. Referring to the complementary TEM dimension measurements, the former (17.9 ± 0.5 nm) corresponds to the width of the twisting ribbon, and the latter (11.2 ± 0.5 nm) corresponds to the thickness of the ribbon. From XRD, the height value of the C_{12}−Aβ(11−17) bilayer is about 4.0 nm (Figure S1 in the Supporting Information), which might be a little smaller than the value in aqueous solution because of the drying states. Therefore, the ribbon with a thickness of ∼11 nm might comprise two bilayer units and a gap filled with water molecules and counterions between them. Similar structure has been reported for chiral gemini surfactant 16−2−16.[34] Such a kind of bilayer structure has not been found in the C_{12}−Aβ(11−17) sample at pH 3.0 by XRD.

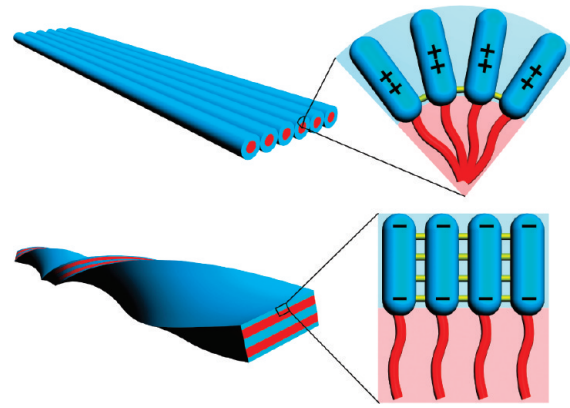

Figure 6. Schematic illustration of the intermolecular interaction within the C_{12}−Aβ(11−17) self-assemblies at pH 3.0 (top) and pH 10.0 (bottom). Yellow dashes represent hydrogen bonds.

The variation in fibril morphology at different solvent conditions should arise from the different manners of the intermolecular interactions within the self-assemblies, as illustrated in Figure 6. At pH 3.0, the hydrogen bond could form only between the residues next to the alkyl tails, and the outer part of the peptide moiety adopts the secondary structure of a flexible random coil. The two positive imidazolyl groups in the middle of the peptide increase the electrostatic repulsion between the neighboring head groups. Hence, the peptide−amphiphile molecules may organize into a cylinder with relatively high curvature. Moreover, the micelle surface is covered by neutral residues, which could lead to further aggregation of the cylindrical micelles into nanotapes through lateral association. Differently, at pH 10.0 the two negative carboxyl groups separate apart and the one at the terminal of the molecule is rather flexible, which weakens the intermolecular repulsion. The peptide moiety adopts a β-sheet conformation and the high extent of hydrogen bonding could drag the head groups closer. Thus, the curvature of the self-assembly is greatly reduced to a flat bilayer structure. Previous studies reported that amyloid polymorphism could arise from the variation in hydration states of the peptide,[36] the molecular conformation and packing within each protofilament,[37−39] and lateral association manners between protofilament units,[40,41] where many questions still remain unanswered.[42] Here, the results provide additional proof of the fibril polymorphism, and the proposed mechanism underlying the morphological variation of C_{12}−Aβ(11−17) self-assemblies with pH may be helpful for understanding the molecule-level structural basis of amyloid fibril polymorphism.

Conclusions

The self-assembly of peptide−amphiphile C_{12}−Aβ(11−17) in aqueous solution has been studied in comparison with amyloid β-peptide fragment Aβ(11−17). Aβ(11−17) is generally a hydrophilic peptide sequence and is not able to assemble into characteristic amyloid fibrils as other Aβ fragments. By introduction of a long alkyl chain to the N-terminal of this sequence, the created peptide−amphiphile C_{12}−Aβ(11−17) displays the prominent biological features of Aβ(1−40) in the morphology of the self-assemblies, such as rodlike fibrils, fibril bundles, and twisted ribbons, varying with pH condition. It implies the great importance of the hydrophobic interaction exerted upon amyloid fibrillogenesis and the significance of solvent condition on the amyloid polymorphism. Additionally, this work may help to guide the design of biomaterial scaffoldings by inscribing biological signals in the self-assemblies.

Acknowledgment. We are grateful for financial support from the National Natural Science Foundation of China and National Basic Research Program of China (Grants 20633010, 2005cb221300). We gratefully acknowledge the Institute of Biophysics of the Chinese Academy of Sciences for access to the transmission electron microscope (FEI Tecnai 20).

Supporting Information Available: XRD spectra at pH 3.0 and 10.0, pH titration curve, and AFM image of the twisted fibrils at pH 10.0 in nine-color table form. This material is available free of charge via the Internet at http://pubs.acs.org.

References and Notes

(1) Whitesides, G. M.; Boncheva, M. *Proc. Natl. Acad. Sci. U.S.A.* **2002**, *99*, 4769.
(2) Zhang, S.; Marini, D. M.; Hwang, W.; Santoso, S. *Curr. Opin. Chem. Biol.* **2002**, *6*, 865.
(3) Aggeli, A.; Bell, M.; Boden, N.; Keen, J. N.; McLeish, T. C. B.; Nyrkova, I.; Radford, S. E.; Semenov, A. *J. Mater. Chem.* **1997**, *7*, 1135.
(4) Silva, h. A.; Czeisler, C.; Niece, K. L.; Beniash, E.; Harrington, D. A.; Kessler, J. A.; Stupp, S. I. *Science* **2004**, *303*, 1352.
(5) Hartgerink, J. D.; Beniash, E.; Stupp, S. I. *Science* **2001**, *294*, 1684.
(6) Holmes, T. C.; Lacalle, S. d.; Su, X.; Liu, G.; Rich, A.; Zhang, S. *Proc. Natl. Acad. Sci. U.S.A.* **2000**, *97*, 6728.
(7) Zhang, S.; Holmest, T.; Lockshin, C.; Rich, A. *Proc. Natl. Acad. Sci. U.S.A.* **1993**, *90*, 3334.
(8) Lu, K.; Jacob, J.; Thiyagarajan, P.; Conticello, V. P.; Lynn, D. G. *J. Am. Chem. Soc.* **2003**, *125*, 6391.
(9) Hong, Y.; Legge, R. L.; Zhang, S.; Chen, P. *Biomacromolecules* **2003**, *4*, 1433.
(10) Zhang, S. *Biotechnol. Adv.* **2002**, *20*, 321.
(11) Paramonov, S. E.; Jun, H.-W.; Hartgerink, J. D. *J. Am. Chem. Soc.* **2006**, *128*, 7291.
(12) Yamada, N.; Komatsu, T.; Yoshinaga, H.; Yoshizawa, K.; Edo, S.; Kunitake, M. *Angew. Chem., Int. Ed.* **2003**, *42*, 5496.
(13) Ganesh, S.; Prakash, S.; Jayakumar, R. *Biopolymers* **2003**, *70*, 346.
(14) Yamada, N.; Ariga, K.; Naito, M.; Matsubara, K.; Koyama, E. *J. Am. Chem. Soc.* **1998**, *120*, 12192.
(15) Adams, D. J.; Holtzmann, K.; Schneider, C.; Butler, M. F. *Langmuir* **2007**, *23*, 12729.
(16) Maltzahn, G. v.; Vauthey, S.; Santoso, S.; Zhang, S. *Langmuir* **2003**, *19*, 4332.
(17) Vauthey, S.; Santoso, S.; Gong, H.; Watson, N.; Zhang, S. *Proc. Natl. Acad. Sci. U.S.A.* **2002**, *99*, 5355.
(18) Marini, D. M.; Hwang, W.; Lauffenburger, D. A.; Zhang, S.; Kamm, R. D. *Nano Lett.* **2002**, *2*, 295.
(19) Dong, H.; Paramonov, S. E.; Aulisa, L.; Bakota, E. L.; Hartgerink, J. D. *J. Am. Chem. Soc.* **2007**, *129*, 12468.
(20) Dexter, A. F.; Middelberg, A. P. J. *J. Phys. Chem. C* **2007**, *111*, 10484.
(21) Nilsson, G.; Gustafsson, M.; Vandenbussche, G.; Veldhuizen, E.; Griffiths, W. J.; Sjövall, J.; Haagsman, H. P.; Ruysschaert, J.-M.; Robertson, B.; Curstedt, T.; Johansson, J. *Eur. J. Biochem.* **1998**, *255*, 116.
(22) Hartgerink, J. D.; Beniash, E.; Stupp, S. I. *Proc. Natl. Acad. Sci. U.S.A.* **2002**, *99*, 5133.
(23) Stendahl, J. C.; Rao, M. S.; Guler, M. O.; Stupp, S. I. *Adv. Funct. Mater.* **2006**, *16*, 499.
(24) Dexter, A. F.; Middelberg, A. P. J. *Ind. Eng. Chem. Res.* **2008**, *47*, 6391.
(25) Clippingdale, A. B.; Wade, H. D.; Barrow, C. J. *J. Peptide Sci.* **2001**, *7*, 227.
(26) Janek, K.; Rothemund, S.; Gast, K.; Beyermann, M.; Zipper, J.; Fabian, H.; Bienert, M.; Krause, E. *Biochemistry* **2001**, *40*, 5457.
(27) Marcinowski, K. J.; Shao, H.; Clancy, E. L.; Zagorski, M. G. *J. Am. Chem. Soc.* **1998**, *120*, 11082.
(28) Wood, S. J.; Wetzel, R.; Martin, J. D.; Hurle, M. R. *Biochemistry* **1995**, *34*, 724.
(29) Danielsson, J.; Jarvet, J.; Damberg, P.; Gräslund, A. *Biochemistry* **2004**, *43*, 6261.
(30) Balbach, J. J.; Ishii, Y.; Antzutkin, O. N.; Leapman, R. D.; Rizzo, N. W.; Dyda, F.; Reed, J.; Tycko, R. *Biochemistry* **2000**, *39*, 13748.
(31) Wang, J.; Zhu, S.; Xu, C. *Biochemistry, Third Edition*; Advanced Education Press: Beijing, 2002.
(32) Cao, M.; Han, Y.; Wang, J.; Wang, Y. *J. Phys. Chem. B* **2007**, *111*, 13436.
(33) Behanna, H. A.; Donners, J. J. J. M.; Gordon, A. C.; Stupp, S. I. *J. Am. Chem. Soc.* **2005**, *127*, 1193.
(34) Oda, R.; Artzner, F.; Laguerre, M.; Huc, I. *J. Am. Chem. Soc.* **2008**, *130*, 14705.
(35) Baumann, M. K.; Textor, M.; Reimhult, E. *Langmuir* **2008**, *24*, 7645.
(36) Dzwolak, W.; Grudzielanek, S.; Smirnovas, V.; Ravindra, R.; Nicolini, C.; Jansen, R.; Loksztejn, A.; Porowski, S.; Winter, R. *Biochemistry* **2005**, *44*, 8948.
(37) Petkova, A. T.; Leapman, R. D.; Guo, Z.; Yau, W.-M.; Mattson, M. P.; Tycko, R. *Science* **2005**, *307*, 262.
(38) Madine, J.; Jack, E.; Stockley, P. G.; Radford, S. E.; Serpell, L. C.; Middleton, D. A. *J. Am. Chem. Soc.* **2008**, *130*, 14990.
(39) Radovan, D.; Smirnovas, V.; Winter, R. *Biochemistry* **2008**, *47*, 6352.
(40) Goldsbury, C.; Frey, P.; Olivieri, V.; Aebi, U.; Müller, S. A. *J. Mol. Biol.* **2005**, *352*, 282.
(41) Uversky, V. N.; Kabanov, A. V.; Lyubchenko, Y. L. *J. Proteome Res.* **2006**, *5*, 2505.
(42) Kodali, R.; Wetzel, R. *Curr. Opin. Struct. Biol.* **2007**, *17*, 48.

JP904289Y